Journal of Cave and Karst Studies, v. 88, nos. 1/2, p. 1-18. DOI: 10.4311/2025ES0114

MULTI-PHASE HYPOGENE SPELEOGENESIS: THE BOPPER CAVE SYSTEM, GRAND CANYON, USA

Sierra Heimel[1,2,C], Benjamin Tobin[2,3], and Georgina Lukoczki[2]

Abstract

The Bopper Cave System (BCS) in the Grand Canyon, USA, offers a unique case study in multi-phase hypogene speleogenesis. The BCS, discovered in 2006, presents distinct features differing from other hypogene caves regionally yet sharing similarities with sulfuric acid caves globally. We hypothesize that the formation of the BCS involves multiple hypogene fluids varying in origin, composition, and timing. Field observations and mineralogical analyses support this, revealing four stages of speleogenesis: dissolution of the network maze cave (likely by CO_2-rich waters), fluctuation in the water table and subsequent fluid chemistry change resulting in deposition of Fe–Mn oxides, lowering of the water table and subsequent speleogenetic (replacement) gypsum rind deposition and speleogen development (likely by SO_4-rich waters), and a transition to vadose conditions followed by secondary sulfate and carbonate deposition. These stages, driven by shifting hydrogeologic conditions, have resulted in the diverse morphology and mineralogy observed in the BCS. Our findings, when added to regional cave development models, suggest localized variability in speleogenetic processes driven by hypogene fluids that led to the formation of the BCS. This study underscores the complexity of hypogene speleogenesis and the need for more nuanced models to account for spatial and temporal variability in fluid chemistry.

INTRODUCTION

In the United States, the understanding of hypogene speleogenesis has grown as studies have begun applying the concept of speleogenesis to karst regions across diverse physiographic provinces (Hill, 1990; Palmer et al., 2016). As recognition of the widespread influence of hypogene processes on karst systems has evolved, the broader need to document hypogene fluid behaviors and complexities in karst literature has become more evident (DuChene et al., 2017; Gulley and Polk, 2017; Tennyson et al., 2017; Burgess, 2021; Hose et al., 2021).

While the dominant models in hypogene speleogenesis describe cave formation via fluids rich in sulfate (SO_4) (De Waele et al., 2024) or carbon dioxide (CO_2) (Spötl et al., 2016), these models often assume a single, stable fluid source throughout the cave-forming process. This simplification may overlook the dynamic and potentially variable nature of fluid contributions over time, including shifts in geochemical composition, tectonic processes, or hydrological connectivity. As a result, such models might not fully capture the complexity of subsurface environments, where fluids derived from different sources, each with distinct chemical signatures, can alternate or interact with bedrock in deep confined aquifers, influencing dissolution patterns and overprinting mineral deposits in more intricate ways than previously accounted for. Previous studies of Grand Canyon hypogene caves included smaller caves, which were likely dissected components of larger systems unknown at the time (Polyak et al., 2008). The Bopper Cave System (BCS) allows for the study of a large and more complete cave system.

This focus on a singular fluid origin overlooks the dynamic nature of fluid interactions across spatial and temporal scales, which has been well-documented in geologic research outside karst environments (e.g., Bucher and Stober, 2010; Pegler et al., 2014). Research has demonstrated that the spatial and temporal heterogeneity of speleogenetic fluids is intrinsically linked to regionally variable tectonic processes, highlighting how shifts in geological dynamics influence fluid migration and chemistry over time (Huntoon, 1996). Such variability, observed from diagenesis to present-day hydrological patterns, underscores the complexity inherent in cave development (Klimchouk et al., 2017) and challenges the assumption of uniform fluid sources in hypogene systems. Notably, research from the Colorado Plateau physiographic region has emphasized the complexity of tectonic evolution in the region and the interaction of multiple fluids with differing chemistries moving through confined aquifers and permeable strata over time (Wenrich and Sutphin, 1989; Huntoon, 1996; Crossey et al., 2006).

Despite significant advancements in the identification and interpretation of hypogene cave systems over the last half century, critical gaps remain in understanding the role of these varying fluid chemistries in cave development, especially as they relate to regionally variable tectonic processes. Only recently in the karst literature have spatially and temporally

[1]National Park Service, Oregon Caves National Monument and Preserve, 21000 Caves Hwy, Cave Junction, OR 97523
[2]Kentucky Geological Survey, University of Kentucky, 310 Columbia Ave., Lexington, KY 40506
[3]National Cave and Karst Research Institute, New Mexico Tech, Carlsbad, NM 88220
[C]Corresponding author: sierra_heimel@nps.gov.

heterogeneous fluids been considered to play a major role in speleogenesis (Columbu et al., 2021). This is particularly applicable within hypogene systems with polygenetic origins, inactive hypogene caves, or those obscured by secondary epigenetic features, which often complicate interpretations (Farrant and Harrison, 2017; Klimchouk et al., 2017; Spötl et al., 2017).

Previous hypogene speleogenesis models have suggested a relatively uniform speleogenetic framework dominated by CO_2-rich fluids for hypogenic karst in the Grand Canyon. Observations from the BCS, an inactive hypogene cave in the Grand Canyon, suggest that this model is incomplete. Using evidence from cave mineralogy and morphologic features, we assess the hypothesis that hypogene speleogenesis in the Grand Canyon reflects spatial and temporal heterogeneity in the origin and composition of hypogene fluids and processes.

STUDY SITE

The Grand Canyon of northwestern Arizona is located on the western edge of the Colorado Plateau physiographic region of the United States (Fig. 1), a tectonically active region characterized by thick continental crust (Karlstrom et al., 2022). The term hypogene speleogenesis was first applied to the phreatic caves in the Grand Canyon by Hill and Polyak (2010) and was also the first mention of hypogene speleogenesis on the Colorado Plateau. Huntoon (2000a) referred to these caves as artesian. The BCS was discovered in 2006 and was recognized as an inactive hypogene cave with unique minerals and cave formations that had never been described in hypogene caves before (Tobin et al., 2021).

Geologic Setting

The Grand Canyon showcases over 1.6 billion years of geological history, most of which is exposed by stratigraphic units from the lower Proterozoic Vishnu Basement Rocks to the upper Permian Kaibab Formation. Key stratigraphic units include the Cambrian Tapeats Sandstone and Bright Angel Shale, which represent the base of the Paleozoic section and indicate ancient marine environments. These are overlain by the regionally important carbonate sequence of the Redwall–Muav (RM) aquifer, comprising the Cambrian Muav Limestone, the Devonian Temple Butte Formation, and the Mississippian Redwall Limestone (Huntoon, 1974). The sedimentary units were deposited in shallow marine and fluvial environments, which laid the groundwork for fluid interactions influencing the formation of the region's extensive cave systems (Kent and Rawson, 1980). The stratigraphic units above the Redwall Limestone comprise a suite of sedimentary layers, representing a variety of marine and terrestrial environments deposited through the end of the Paleozoic era.

The tectonic evolution of the Colorado Plateau has dramatically influenced its geology and hydrology. The uplift of the Mogollon Highlands during the Triassic period redirected fluid pathways and altered the chemistry of infiltrating waters (Huntoon, 1996). Uplift during the Laramide Orogeny, approximately 60 million years ago, elevated the landscape and modified groundwater flow patterns. Uplift of the Colorado Plateau is debated and poorly constrained, but it is generally described as occurring in three phases since the Cretaceous, with rates increasing through time (Roberts et al., 2012). Incision rates of the Colorado River in the Grand Canyon are used to estimate uplift and indicate steady long-term incision that varies spatially from east to west, consistent with migrating mantle buoyancy and uplift from Neogene volcanism (Roberts et al., 2012; Crow et al., 2014).

Moreover, the volcanic history of the Grand Canyon region is marked by episodes of volcanic activity that have contributed to its geological complexity. Quaternary volcanic features, including composite lava dams, indicate recent volcanic processes occurring in the Grand Canyon region (Crow et al., 2008). Today, evidence of neotectonic activity and mantle-derived gases can be seen in the geochemical signatures of modern springs (Crossey et al., 2009). Breccia pipes, which are vertical, cylindrical features formed from the collapse of overlying sediments into the underlying Redwall Limestone, serve as crucial conduits for both hydrothermal fluids and groundwater and were likely mineralized by fluids that interacted with eroding volcanic and Precambrian crystalline rocks in the Triassic Mogollon highlands to the south (Wenrich and Sutphin, 1989).

The combined impact of tectonic uplift and volcanic activity has led to varied spatial and temporal fluid contributions within the Colorado Plateau. This interaction of diverse hydrochemical processes has resulted in a heterogeneous distribution of hypogene fluid contributions to the groundwater, which, in turn, plays a significant role in cave development. The variability in fluid sources and compositions, profoundly influenced by tectonic forces and volcanic activity, underscores the intricate relationships shaping the karst systems of the Grand Canyon.

Karst Development in the Grand Canyon

During the late Mississippian, a regionally widespread karst developed in the newly emergent Redwall Limestone (McKee and Gutschick, 1969; Beus, 1990). Since its formation, this karst has been infilled with sediments, breccias, and cements and is recognized today as a paleokarst system. The Redwall Limestone was reportedly buried to a maximum depth of 5 km (Karlstrom et al., 2014) approximately 250 million years ago and remained deeply buried from the end of the Paleozoic through the beginning of the Cenozoic (Sylvia, 1985). Fractures and faults from the Laramide Orogeny,

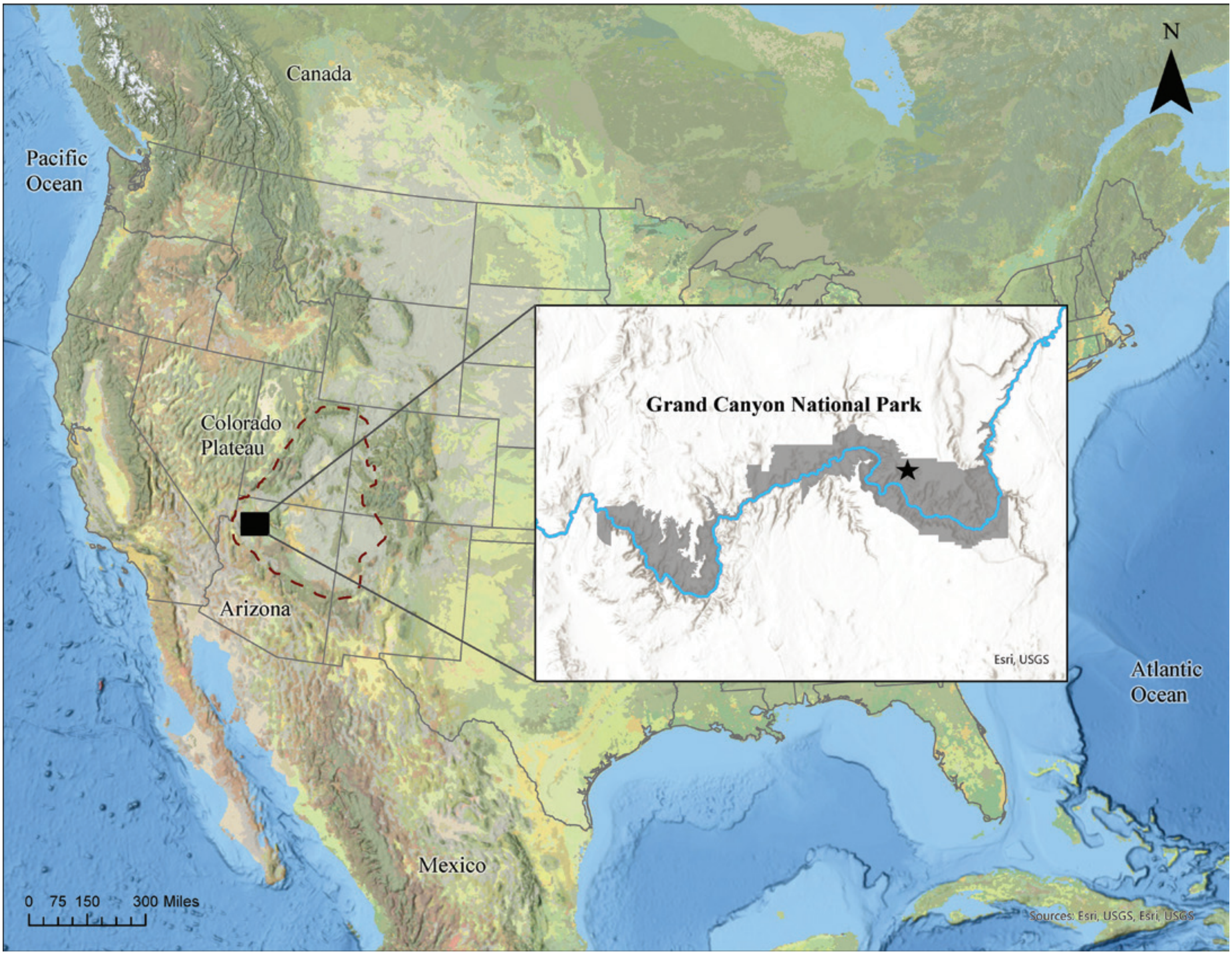

Figure 1. Location of the Bopper Cave System (star) and Grand Canyon National Park (dark gray) within the greater context of the Colorado Plateau, USA.

which uplifted the region approximately 60 million years ago to its current elevation, play a significant role in enhancing permeability within the RM aquifer, especially in the Redwall Limestone (Blakey and Ranney, 2008). Well before the establishment of the BCS, large-scale faults displaced the Redwall Limestone by hundreds of meters, creating zones of increased permeability and cavern development in areas of groundwater circulation (Huntoon, 1974). Recent studies highlight the importance of preferential dissolution of the dolomitic facies in the Mooney Falls Member of the Redwall Limestone, which leads to increased porosity, permeability, and large groundwater storage potential (Dohm, 2017; Heimel, 2019).

Today, an extensive karst system exists in the Redwall and Muav Limestones, with over 500 caves documented and 150 km of surveyed cave passage (Tobin et al., 2021). There are two distinct morphologies of caves in the Grand Canyon: confined (phreatic origin) and unconfined (vadose origin) caves (Huntoon, 2000b). Confined caves were formed in the phreatic zone, below the water table, and are generally found in the Mooney Falls member of the Redwall Limestone (Fig. 2) (McKee, 1963). Prior to the incision of the Grand Canyon and a related drop in the water table, these caves were fully saturated and developed into 2- and 3-dimensional maze caves with generally low hydraulic gradients (Palmer, 1975; Hill and Polyak, 2010) that tend to follow regional structural patterns (Heimel and Tobin, 2022). Unconfined caves have formed since the incision of the canyon and are fed by recharge from precipitation on the rims of the canyon (Jones, 2017). These caves are typically simpler in morphology with steeper hydraulic gradients than confined caves and are often associated with major springs in the canyon (Huntoon, 2000b). Both confined and unconfined systems are associated with regional faults (Tobin et al., 2021).

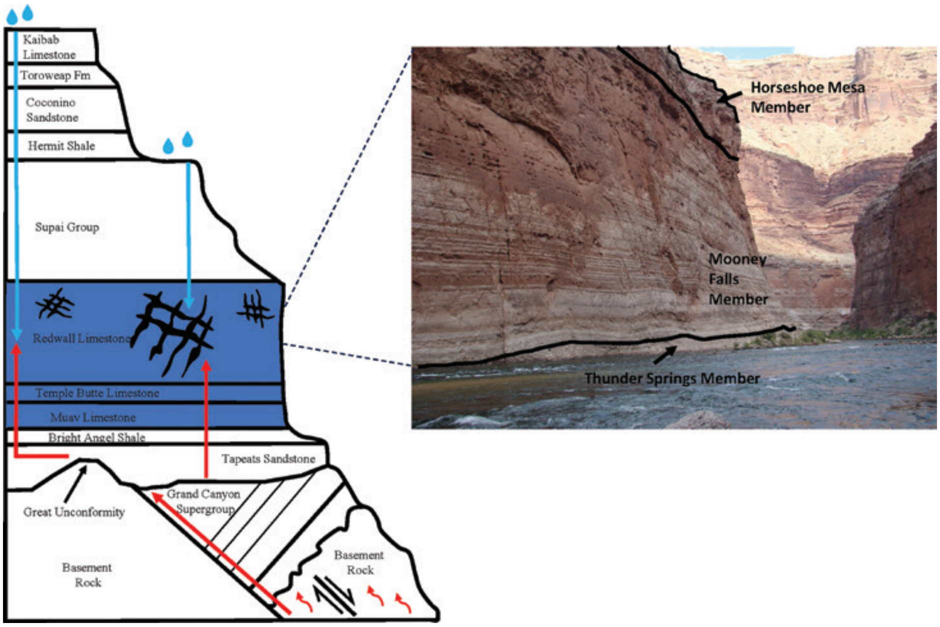

Figure 2. Stratigraphic and speleogenetic setting for cave development in the Redwall–Muav aquifer (shown in dark blue) of the Grand Canyon. Faults and fractures serve as conduits for fluid migration. Epigenic fluids (blue arrows) migrate downward from the rims of the Grand Canyon, and hypogenic fluids (red arrows) migrate upward from deep sources. The inset image is a photograph modified from Dohm (2017) showing the exposed members of the Redwall Limestone in the eastern Grand Canyon; from bottom to top: the Thunder Springs Member at river level, the dolomite-banded Mooney Falls Member, and the overlying Horseshoe Mesa Member. The Mooney Falls Member is approximately 96 m thick in this part of Grand Canyon.

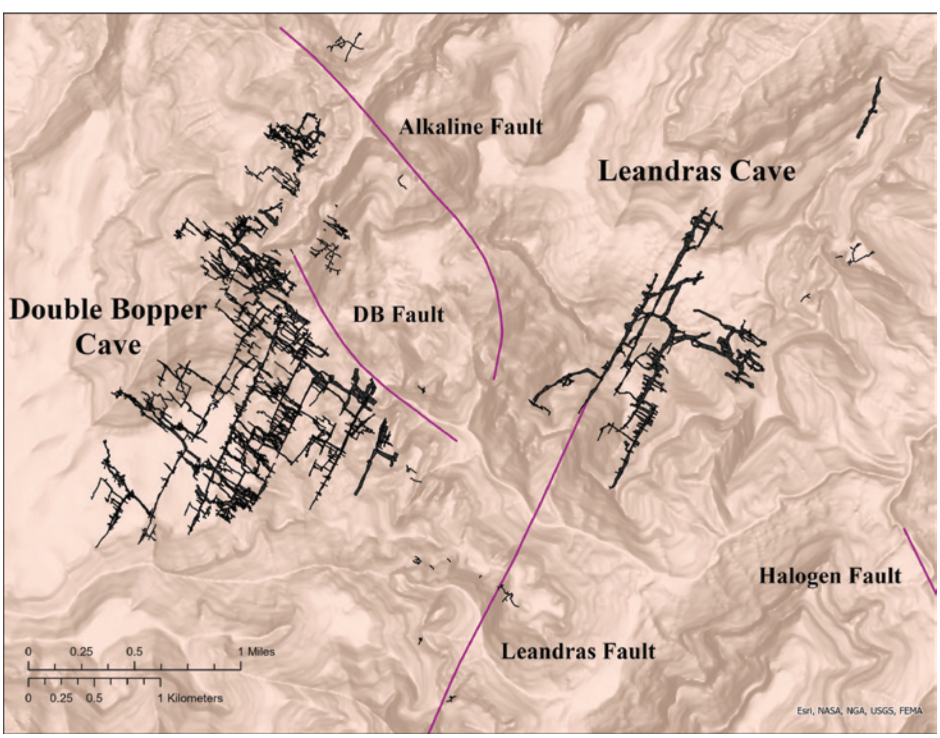

Figure 3. Map of the Bopper Cave System (BCS), including Double Bopper Cave and Leandras Cave along with many other smaller caves (names not shown) that comprise the BCS. Faults are shown in purple.

The Bopper Cave System

The BCS is located in a remote alcove in the upper reaches of the Redwall Limestone on the Kaibab Plateau. The BCS is composed of several distinct caves, including large caves such as Double Bopper and Leandras Caves in addition to many smaller caves (Fig. 3). These caves are crosscut and separated by major side canyons that indicate the caves were once connected before the incision of the Grand Canyon bisected the BCS. The primary cave of focus for this study is Double Bopper. With over 64 km (40 mi) of mapped passage, Double Bopper is the longest cave in the Grand Canyon and, as of 2026, the 13th longest cave in the United States.

The BCS is not associated with modern water flow and is a hypogene network maze cave with a high density of caves and large natural cave entrances (Tobin et al., 2021; Heimel and Tobin, 2022). Passages do not converge as tributaries but instead branch outward from fracture networks (Fig. 3). The network maze of passages in the BCS includes both spongework-type and rectilinear passages as defined by Palmer (1991). The BCS has a large horizontal extent, and the sizes of cave passages vary widely, ranging from tens of meters in diameter to passage widths impassable by humans. The largest passages in the BCS are in the Leandras portion of the BCS and along the trace of the Double Bopper Fault in Double Bopper Cave, with the largest passages having widths over 38 m and lengths of up to 1 km. The smallest passages in the BCS are located at the distal ends of Double Bopper Cave, with large passages narrowing to eventually become too tight for human exploration. Many of the large rooms are zones of breakdown and collapse, with less breakdown present in smaller passages.

The BCS displays no spatial relationship with surface topography on the Kaibab Plateau of the North Rim of the Grand Canyon but has important relationships with the local fracture network and surrounding faults (Heimel and Tobin, 2022). The joint-controlled nature of the cave system is likely a result of tectonic forces and erosional unloading of overburden (Mandl, 2005; Klimchouk, 2009). Thus, the BCS has developed within a complex structural setting with well-developed fracture networks in the Redwall Limestone and four major documented faults proximal to the BCS: the Halogen, Alkaline, Leandras, and Double Bopper Faults (Fig. 3). The Halogen Fault is a high angle normal fault 15 km long with 6–24 m of offset (Billingsley and Hampton, 2000) located over a kilometer away from the BCS, the Leandras fault is a high angle normal fault 4 km long (Billingsley and Hampton, 2000) that intersects major passages of the BCS, the Double Bopper fault sits adjacent to terminating passages in the BCS, and the Alkaline Fault is located between the Leandras and Double Bopper Caves and sits adjacent to smaller caves in the BCS. Passage size statistically decreases with increasing distance from the Halogen and Leandras faults, suggesting their role as conduits for aggressive hypogene fluids that enhanced dissolution near the faults, while the inverse relationship with the Double Bopper fault suggests it acted as a barrier to speleogenetic fluids (Heimel and Tobin, 2022). These relationships, however, are complex, and additional controls such as fracture permeability and lithologic variability also influence passage size. Additionally, there are smaller faults expressed and documented more recently from within the BCS, such as the Green Door Fault (Heimel, 2022) (Fig. 4).

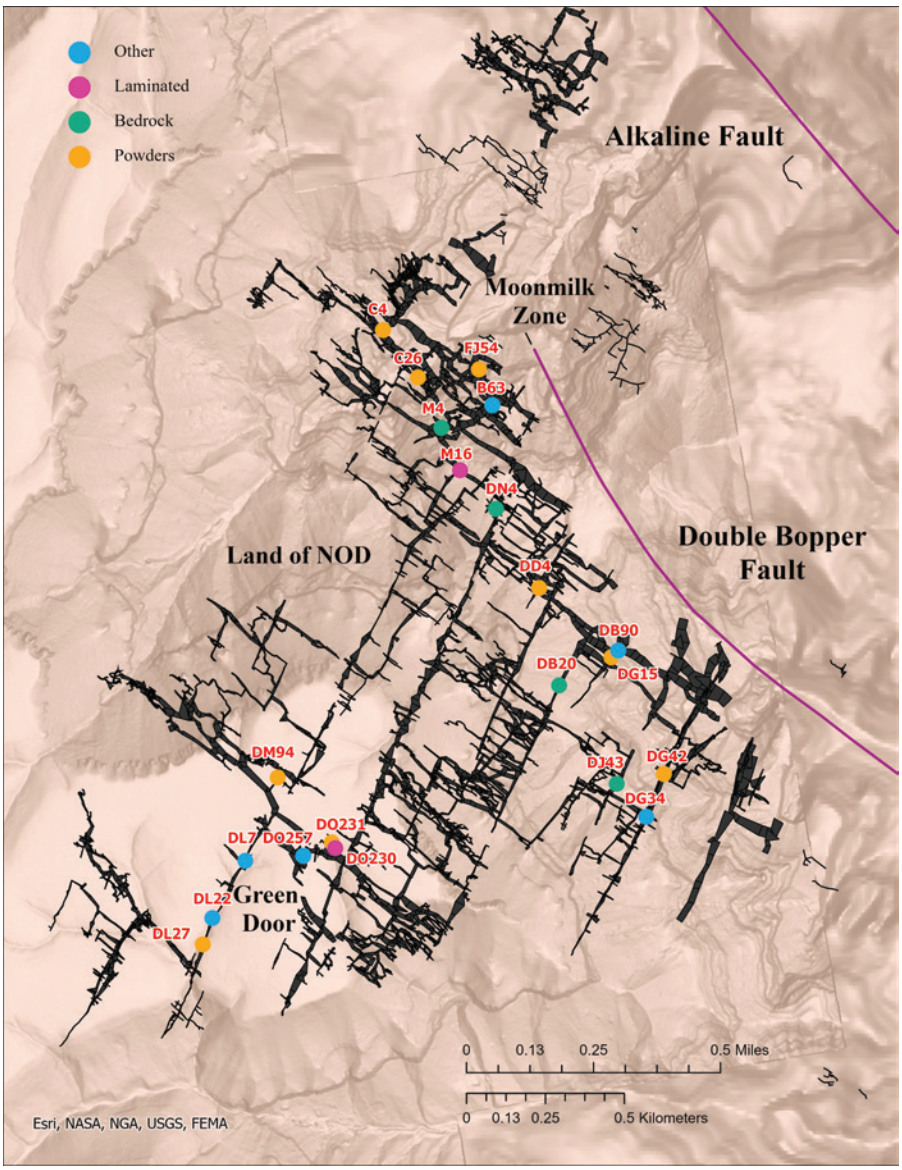

Figure 4. Sampling locations for X-ray diffraction analysis in the Double Bopper portion of the Bopper Cave System. The colored circles represent the types of samples analyzed: powdered deposits are orange, bedrock samples are green, laminated deposits are pink, and samples that do not fall into the preceding categories are labeled as “other” and are marked with blue. Three zones mentioned in the text include the Land of NOD, a.k.a Noxious Orange Dust, the Green Door (located at station DO257), and the Moonmilk Zone.

METHODS

Field Observations

We documented geologic field observations to describe the occurrence and types of cave morphologies, speleogens, sediments, secondary deposits, and cave-related structural features. Secondary deposits refer to speleothems and sediments formed after the initial dissolution of the cave system. For each identified feature, we recorded descriptive characteristics and spatial locations using a combination of notes and photographs. For spatial reference, we documented features' locations to the nearest cave survey station. We used photographs to document the scales of features, though some features were photographed occurring in the ceiling of the cave and have no scale.

Sample Collection

Our team spent 4 days underground from October 26 through 29, 2021, collecting 13 bedrock and 85 secondary deposit samples. The collection locations of secondary deposits, intended for broad spatial coverage within the cave, were determined by our travel routes. We selected previously unidentified mineral specimens based on documentation from previous cave resource inventory surveys conducted by citizen scientists. These notes detailed the colors and morphologies of unidentified minerals relative to specific cave survey stations. In our sampling approach, we focused on obtaining at least one specimen of each type of unidentified mineral. To minimize impact to the cave, mineral and speleothem samples were limited to those that had fallen to the cave floor whenever possible.

Figure 5. (a) Circular passage morphology with post-speleogenetic breakdown and collapse. Caver in the center of the photo for scale. Photo by Stephen Eginoire. (b) Lens-shaped morphology with post-speleogenetic breakdown and collapse. Prominent iron-red, stratiform, block-like breccia on the left side of the photo. The extent of the breakdown is unknown. Photo by James Hunter.

X-Ray Diffraction

Of the nearly 100 samples we collected, 22 were analyzed for mineral composition (Fig. 4) by powder X-ray diffraction (XRD) using a Bruker D8 DISCOVER equipped with a Bruker scintillation counter detector with CuKα radiation (X-ray tube operated at 40 kV and 40 mA) at the Kentucky Geological Survey, University of Kentucky. Data were collected in the angular range of 2°–70° 2θ with a 0.02° step size and <1 s counting time per step. We identified mineral phases using the Bruker DIFFRAC.EVA software version 5.2 with powder diffraction database version PDF 2-2021.

RESULTS

Morphology

The BCS exhibits a variety of phreatic morphologies, including large lens-shaped and circular passages (Fig. 5). Extensive post-speleogenetic breakdown and collapse are evident in large passages, obscuring the lower half of the cave passages. This may conceal rift-shaped floors, which are a common morphology associated with hypogene speleogenesis. Passages in the BCS are generally horizontal, with an average dip of 2° to the south, matching the regional dip of the Mooney Falls Member of the Redwall Limestone. Smaller cave passages and passages in close proximity to faults are irregular in shape. The vertical extent of the cave reaches 30 m due to one fissure passage in Double Bopper that breaches down into the Thunder Springs Member of the Redwall Limestone. This is the only reported occurrence of cave development in the chert-banded Thunder Springs Member in Grand Canyon. Morphologies typical of vadose caves, such as shafts, canyons, or dome and pit complexes, have not been documented in Double Bopper.

Speleogens

Speleogens found in the BCS consist of cupolas, air scallops, solution domes, pendants, ceiling half tubes, and acid pool basins with rillenkarren. Variously sized cupolas dot the ceiling and adjacent walls in many passages and do not follow visible fractures (Fig. 6). Air scallops are micro cupolas and are abundant in the BCS. Pendants are found in the BCS in many locations and are likely either breccia or other insoluble bedrock residues left behind after selective dissolution in the cave passage (Fig. 7). Ceiling half tubes are not as common as phreatic tubes in the BCS but are seen at several locations (Fig. 8). Solution domes are larger than cupolas and are found in the ceiling of many larger passages in the BCS, with some ceiling domes reaching over 15 m high (Fig. 9). Wall channels with rillenkarren are found in isolated locations and may represent relic acid pool basins with rillenkarren marking the top edge of a pool in the BCS. There are no speleogens typical of vadose caves documented in the BCS, such as solution scallops or anastomoses.

Secondary Deposits and Speleothems

Colorful secondary deposits are abundant throughout the cave and include a diverse range of speleothems and sediments. These deposits consist of various minerals, including sulfates, carbonates, Fe–Mn oxides, a phosphate mineral, and quartz (Table 1).

The largest passages in the cave are associated with the main entrance series near the Double Bopper Fault and are predominantly filled with buff-colored breakdown boulders. Stalagmites and stalactites have only been documented in the BCS proximal to this fault. Moving away from the Double Bopper Fault, passages become drier and coated in gypsum occurring as corkscrew-shaped “flowers,” “swords,” “chandeliers,” “grass,” and “hair” (Figs. 10–12, DG34 and DB90 in Table 1). In those areas of the BCS where the cave walls are not decorated with secondary deposits or

Figure 6. Extensive cupola and air scallop development on the “pocketed” cave walls in a fissure passage. Photo by Stephen Eginoire.

Figure 7. A large, isolated ceiling pendant speleogen impregnated with Fe–Mn oxides. Photo by James Hunter.

Figure 8. Ceiling half tube in a lens-shaped passage with gypsum flowers extruding from the walls and ceiling. Photo by Stephen Eginoire.

Figure 9. Vertical ceiling dome with cupola and air scallops outlining the dome. Photo by Stephen Eginoire.

speleothems, the bedrock is highly friable and bleached white with hues of orange and red (Fig. 14). Laterally continuous breccia layers are common in the BCS and consist of brecciated blocks of limestone embedded in yellow and red clays (Figs. 10 and 11). Gypsum also preferentially extrudes from some of these breccia layers, often highlighting alternating layers of the bedrock (Fig. 11).

Table 1. Description and mineralogy of samples analyzed by X-ray diffraction.

Sample ID	Sample Type	Sample Description	Minerals Identified
C4	Powder	Brown powder	Goethite—$Fe(OH)O$
C26	Powder	White powder	Hydromagnesite—$Mg_5(CO_3)_4(OH)_2{\cdot}4H_2O$
DM94	Powder	Orange powder	Hematite—Fe_2O_3
DO231	Powder	Black powder	Manganese oxide—Mn_2O_3
B63	Other	Green translucent coating around boxwork	Gypsum—$CaSO_4{\cdot}2H_2O$, brushite—$CaPO_3(OH){\cdot}2H_2O$
DL27-1	Powder	White powder	Thenardite—Na_2SO_4
DD4	Powder	Yellow powder	Jarosite—$KFe_3(SO_4)_2(OH)_6$, natrojarosite—$NaFe_3(SO_4)_2(OH)_6$
DL22-2	Other	Gypsum foam	Gypsum
DL7	Other	Flower on gypsum foam	Gypsum
DG34	Other	Yellow nodule	Gypsum, calcite—$CaCO_3$, epsomite—$MgSO_4{\cdot}7H_2O$
DG42-1	Powder	Yellow-brown powder	Quartz—SiO_2, gypsum
M4	Bedrock	Purple fine-grained laminated sedimentary rock	Quartz, hematite
DB90-2	Other	Gypsum foam and coating	Anhydrite—$CaSO_4$, quartz
DO257-1	Other	Green-blue botryoidal mineral	Malachite—$Cu_2CO_3(OH)_2$, calcite
DG15	Powder	Yellow powder	Gypsum, jarosite
DB20-3	Bedrock	Red bedrock limestone	Calcite, quartz
DO257	Other	Gypsum foam	Calcite, gypsum
FJ54	Powder	White powder	Epsomite, mirabilite—$Na_2SO_4{\cdot}10H_2O$
DJ43	Bedrock	Crystalized bedrock	Gypsum, dolomite—$CaMg(CO_3)_2$
DO230	Laminated	Brown-yellow powder	Goethite
M16-2	Laminated	Red powder	Hematite
DN4	Bedrock	Green fine-grained bedrock sedimentary rock	Dolomite, calcite

Throughout the cave there are also crusts, rinds, and powder deposits. Crusts occur as coatings up to a few centimeters thick around the rims on breakdown rocks, bedrock, and other secondary deposits. Crusts are typically white and were identified as gypsum and dolomite. Massive, somewhat botryoidal white rinds of 5–10 cm thickness coat the walls, floor, and ceiling in the BCS and were identified as gypsum (DB90-2, Table 1). A small but vibrant green-yellow crusty nodule was observed in one locality in the cave and was identified as epsomite (DG34, Table 1 and Fig. 12).

The sampled powders are fine-grained, porous, lightweight, varied in color, and found as piles or layers on the floor. Piles of white powder are common near gypsum speleothems in the BCS and were identified as thenardite, epsomite, and mirabilite (FJ54 and DL27-1, Table 1). Bright yellow piles of powder found coating a cluster of red breakdown blocks on the floor were identified as jarosite and natrojarosite (DD4, Table 1). The source of this deposit appears to be a 5 cm diameter mineralized zone in the ceiling. Another pile of yellow-brown powder was identified as quartz and gypsum (DG42-1, Table 1). One cave passage, designated as the Moonmilk Zone (Fig. 4), spans approximately 15 m in width and 40 m in length and was found to be blanketed with a 25–30 cm thick layer of white powder, identified as hydromagnesite (C26, Table 1). The source of this deposit appears to be an irregular fracture network of white mineralized veins in the ceiling directly above this passage.

The central portions of the BCS, furthest from entrances and near the center of the network maze cave, display increasing amounts of red, orange, yellow, brown, and black consolidated powders, identified as hematite, goethite, and manganese oxides hereinafter referred to as Fe–Mn oxides (C4, DM94, DO230, DO231, M16-2 in Table 1). Fe and Mn oxides are found primarily in lightweight deposits up to 25 cm thick on the floors and as porous, multicolored coatings on walls and breakdown. Some of the powders form semi-rectangular or circular blocks, and some are laminated (Fig. 13). Disturbance of the consolidated powders results in aerosolization of the fine sediments, thus a section of the BCS is satirically named “The Land of NOD,” a.k.a Noxious Orange Dust. There are some passages where the Fe–Mn oxides and sulfate deposits have peeled away from the cave walls, exposing the friable and bleached bedrock (Fig. 14). A green clayey-looking material was also documented in the exposed bedrock in this section of the cave, which was identified as dolomite and calcite (DN4, Table 1).

Figure 10. A corkscrew-shaped gypsum flower (approximately 25 cm long) extruding from a breccia layer in the Bopper Cave System. Photo by Sierra Heimel.

Figure 11. Gypsum flowers preferentially extruding from horizontal breccia layers in the Mooney Falls Member. Photo by Dave Bunnell.

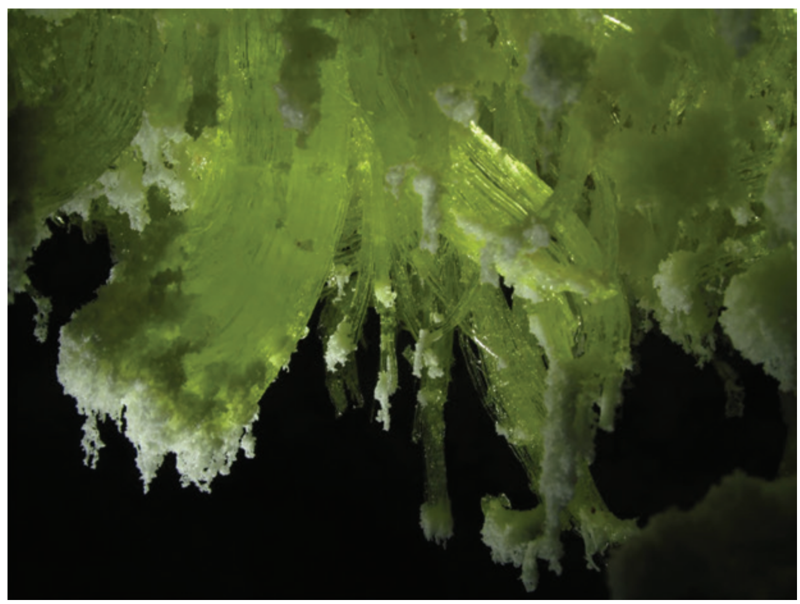

Figure 12. Light green sulfate minerals, likely a combination of epsomite and gypsum. Photo by Paul Burger.

Passages near the Green Door zone (Fig. 4) occur along an unmapped fault. A zone of mineralization with botryoidal green and blue minerals is found here. A sample collected here was identified as malachite (DO257-1 in Table 1 and Fig. 15). Azurite is commonly found with malachite and is likely the blue mineral found in association with malachite but was not differentiated by our XRD analysis. The malachite mineralization was found in association with massive calcite and Fe–Mn oxides in the fault plane. Large, approximately 10 cm long scalenohedral dogtooth calcite spar crystals were found in a cavity in the Green Door zone but not in the fault plane (Fig. 16). Mammillary calcite formations have not been documented in Double Bopper; however, Leandras is documented to contain localized mammillary formations.

The most unique secondary deposits found in the BCS are lightweight, froth- or foam-like deposits made up of gypsum, calcite, and anhydrite (sample DL22-2, Table 1) and are henceforth referred to as gypsum foam. These deposits are found in abundance on the walls and floors of select portions of the BCS. Gypsum foam is extremely delicate; however, a hard secondary coating or encasing was observed around a gypsum foam sample, and this coating was identified as quartz with XRD (Fig. 17). A soft green coating on a gypsum foam sample was identified as brushite (sample B63 in Table 1).

DISCUSSION

The wide variety of speleogens, speleothems, and secondary cave deposits observed in the BCS suggests a complex origin, likely resulting from multiple fluids moving through the Redwall Limestone at different times, dissolving the

Figure 13. Autochthonous cave sediments composed of bright yellow, fine-grained, laminated Fe-oxide sediments. Photo by Sierra Heimel.

Figure 14. An exposed section of bleached and friable bedrock (orange and yellow) underneath a layer of Fe–Mn oxides (brown and black) underneath a botryoidal white gypsum rind. Photo by Sierra Heimel.

Figure 15. Botryoidal malachite and calcite mineralization found near the Green Door mineralized fault zone. Photo by Sierra Heimel.

bedrock and depositing hypogene speleothems in the process. Our observations suggest four distinct stages of speleogenetic development that led to the formation of the BCS (Table 2). Consequently, we propose a modified model of hypogene cave development in the Grand Canyon, building on the previous work by Polyak et al. (2017).

Stage 1 of speleogenesis commenced sometime prior to 4 million years ago, predating the incision of the Grand Canyon, when the Redwall Limestone existed within the deep phreatic zone of the ancient RM aquifer (Polyak et al., 2008) (Table 2, Stage 1). We interpret that the horizontal tube passages in the BCS were formed deep in the ancient RM aquifer during a time when hypogene fluid contributions were present. The spatial patterns of maze caves suggest they were created through the simultaneous widening of passages in low-gradient environments (Klimchouk and Ford, 2000; Klimchouk, 2012). Additionally, the spatial patterns of passage size decreasing in relation to distance from faults suggest that large contributions of hypogene fluids may have been episodically sourced from nearby faults, flowing at low gradients toward Double Bopper Cave, further aiding passage development (Heimel and Tobin, 2022). During this initial phase, acidic hypogene fluids altered the cave walls, bleaching and corroding them to a friable texture at depths of several tens of centimeters. These fluids were likely rich in carbonic acid, as previously proposed (Hill and Polyak, 2010), evidenced by locally preserved dogtooth calcite spar mineralization. The presence of this large euhedral dogtooth calcite spar suggests that it could have formed 500 ± 250 m beneath the water table in the deep phreatic zone, where the transition from supercritical to subcritical CO_2 drives both limestone dissolution and calcite precipitation (Decker et al., 2016) with respect to depth, temperature, and the solubility of $CaCO_3$ during the descent of the potentiometric surface as the cave shifts from the solutional zone into the depositional zone (Hill and Polyak, 2010).

Following the initial dissolution processes, *Stage 2* initiated as the water chemistry of the fluids in the conduits changed with the gradual lowering and fluctuation of the potentiometric surface in the ancient RM aquifer (Table 2, Stage 2). This transition is evidenced by the presence of large quantities of Fe–Mn oxides coating the bleached and altered bedrock, along with laminated Fe–Mn oxides in the BCS. Hematite, an iron oxide mineral commonly deposited in caves from thermal waters and under oxidizing conditions, may convert into goethite (Hill and Forti, 1997). Iron and manganese oxides and hydroxides serve as redox indicators (Levy, 2007), favoring transport in fluids in their reduced form at low pH and Eh, and precipitating as Fe–Mn oxides when these variables increase (Palmer and Palmer, 2012). Fluctuations in the pH and Eh of the ancient RM aquifer, likely influenced by changes in the potentiometric surface

Figure 16. Scalenohedral dogtooth calcite spar near the Green Door zone. Photo by Sierra Heimel.

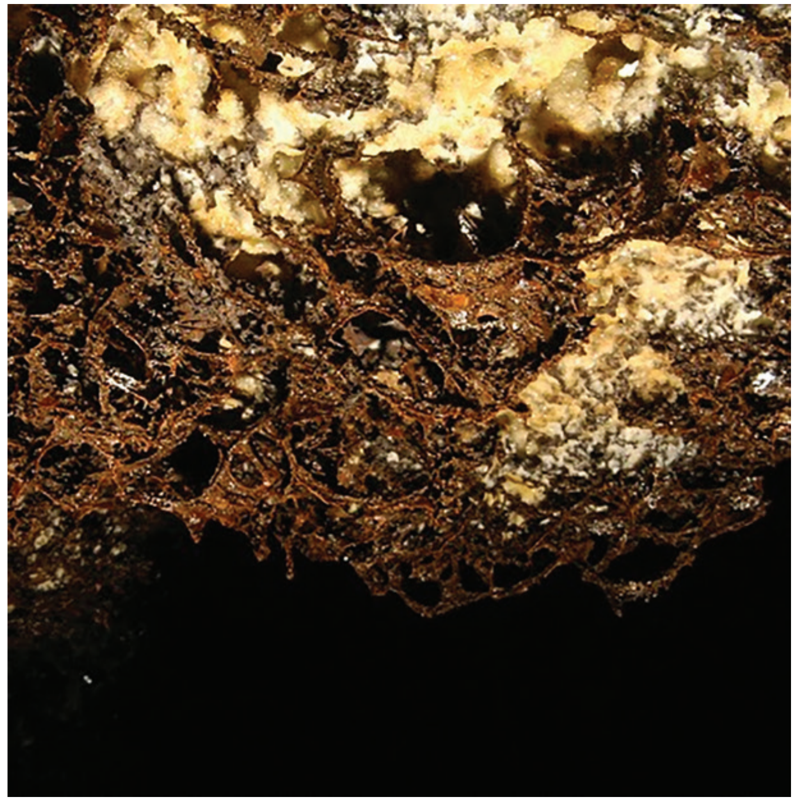

Figure 17. Gypsum foam, made up of anhydrite, gypsum, and quartz (see text for further details). Photo by Stephen Eginoire.

and limestone dissolution, could have led to rising pH levels, promoting the subsequent precipitation of previously soluble iron and manganese as Fe–Mn oxide minerals (Palmer and Palmer, 2012). However, Fe–Mn oxides can also precipitate without a change in pH, particularly when aided by microbial processes (Carmichael et al., 2013). The fine-grained and laminated nature of these sediments indicates that they settled slowly out of the water column in a low-energy environment. The formation of goethite and hematite Liesegang banding likely occurred during Stage 2, with bands representing precipitation lines of iron-rich minerals along groundwater chemical interfaces. These processes are typically the result of numerous precipitation events over long periods of time, with moving groundwater under oxic conditions (Wells et al., 2003).

Additional evidence for Stage 2 is observed in the co-occurrence of Fe–Mn oxides with malachite deposits at the Green Door fault plane, which likely served as a significant fluid pathway. Malachite is typically found in the oxidized upper zones of copper sulfide deposits (Melchiorre and Enders, 2003), where copper-bearing minerals are exposed to groundwater and hydrothermal fluids (Hill and Polyak, 2010). The most likely source of copper in the BCS region is from copper sulfide deposits in breccia pipes (Wenrich, 1985). The carbonate component is likely acquired from CO_2 dissolved in groundwater due to the dissolution of the Paleozoic carbonate bedrock. Therefore, the formation of

Table 2. Speleogenetic stages of the Bopper Cave System.

Stage	Description	Evidence
Stage 1	Initial phreatic conditions with carbonic acid hypogene fluid contributions and early dissolution of limestone.	Abundance of horizontal tube passages, bleached bedrock, and dogtooth calcite.
Stage 2	Changes in water chemistry, rise in pH, and precipitation of Fe−Mn oxides.	Coating and laminations of Fe−Mn oxides, malachite deposit in fault.
Stage 3	Transition to sulfate-dominated fluids, leading to sulfuric acid speleogenesis dominated by dissolution and the formation of replacement gypsum.	Presence of speleogenetic gypsum rinds, distinctive cupolas, air scallops, solution domes, and other features.
Stage 4	Evaporative vadose conditions resulting from water table incision, leading to the deposition of sulfate minerals.	Prolific gypsum deposits, hydromagnesite, and other evaporite minerals.

Table 3. Comparison of conceptual models for hypogene speleogenesis in the Grand Canyon.

Aspect	Polyak et al. (2017) Conceptual Model	BCS Conceptual Model (This Study)
Speleogenetic agents	Dominantly CO_2-rich hypogene fluids; H_2S considered a minor contributor based on limited gypsum abundance.	Multiple hypogene fluids, including CO_2, H_2S, and Cu-rich fluids; sulfuric acid plays a major role during at least one speleogenetic phase.
Role of sulfuric acid speleogenesis (SAS)	Secondary or limited; inferred from a limited gypsum rind and sulfate deposits.	Abundant and locally dominant, evidenced by common gypsum rinds and sulfate mineral assemblages.
Fluid types	Deep-seated hypogene fluids linked to magmatic and/or tectonic activity.	Diverse types of hypogene fluids, including magmatic, tectonic, copper-bearing fluids; contribution of various fluid types varies spatially.
Hydrologic controls	Regional water table fluctuations control dissolution and mineral paragenesis.	Water table position important; episodic interplay with fault-controlled flow paths creates locally unique geochemical conditions and mineral paragenesis.
Predicted speleogenetic sequence	Fe and Mn oxides → calcite spar linings → mammillary calcite → folia → cave rafts → gypsum rinds.	Incomplete or altered sequence with potential overprinting; Fe and Mn oxides → calcite spar linings → mammillary calcite → overprinting and dissolution of most calcite → gypsum rinds → secondary sulfate deposits.
Calcite spar linings	Common and widespread in phreatic passages; used as indicators of formation depth.	Largely absent, suggesting depth estimates based on spar may not apply universally.
Mammillary calcite	Common component of the hypogene mineral assemblage.	Limited or absent in major portions of the BCS.
Gypsum occurrence	Present mainly as late-stage rinds.	Abundant and diverse gypsum formations, indicating sustained sulfuric acid influence.
Cave size vs. completeness of sequence	Larger caves are more likely to preserve the full sequence of hypogene subevents.	The largest cave in the Grand Canyon yet lacks the full predicted sequence.
Conceptual implication	Hypogene caves broadly follow a common evolutionary pathway in the Grand Canyon.	Hypogene speleogenesis is highly heterogeneous; no single model or sequence applies to all Grand Canyon caves.

malachite at the Green Door fault plane likely arises from groundwater interacting with these copper sulfides, migrating upward through the fault structure, and redepositing them as malachite near faults. Although Stage 2 provides suitable conditions for malachite formation, it is also feasible for malachite to precipitate during later stages of speleogenesis as fluid migration patterns evolve, highlighting the complex interactions between geochemical processes and mineral deposition in the Grand Canyon.

Stage 3 (Table 2, Stage 3) subaqueous and subaerial processes took place in a mixed phreatic and vadose environment when the potentiometric surface was at the level of the BCS following a transition to sulfate (SO_4)-dominated fluids at some point, likely prior to the onset of Stage 3, as indicated by the formation of sulfuric acid speleogens (replacement gypsum) in the subaerial zone, just above the water table (Polyak et al., 2017). Speleogenetic (replacement gypsum), a direct product of hypogene processes in the Grand Canyon (Hill and Polyak, 2010), results from the dissolution of limestone by sulfuric acid, accompanied by gypsum co-precipitation (Polyak and Provencio, 2001). Unlike evaporative gypsum, speleogenetic (replacement gypsum) forms thick rinds that are denser and more massive. Observations of massive white rinds, 5–10 cm thick, in combination with XRD analyses, suggest that sample DJ43 contains this type of gypsum, which is common throughout the BCS. This process would have occurred as H_2S migrated upward from deep sources along faults and fractures, interacting with oxygenated water near the BCS subaerial zone, thus producing sulfuric acid and vapor. The resulting sulfate accumulation, along with the calcium from the limestone, would cause gypsum to precipitate on cave surfaces (Palmer, 2007). The sulfuric vapors likely generated buoyant convection currents, with condensation corrosion inducing localized dissolution at the water table interface, resulting in distinctive features such as cupolas, air scallops, solution domes, pendants, ceiling half tubes, and wall channels with rillenkarren (Figs. 6–9). These speleogens are not structurally controlled and do not follow joints or fractures, a trait shared with other large hypogene systems (Galdenzi et al., 2014; De Waele et al., 2024). Some hypogene caves have documented these speleogens forming above structurally controlled feeders (De Waele et al., 2016), but definitive feeders have not been identified in the BCS.

During *Stage 4* (Table 2, Stage 4), as the Colorado River incised the Grand Canyon, the potentiometric surface of the ancient RM aquifer dropped below the level of the BCS, transitioning the cave environment to an entirely evaporative vadose system. This shift resulted in decreased pressure on the cave walls, leading to significant collapse and breakdown of larger conduits. Additional breakdown may also be due to gypsum crystal wedging (White and White, 2003; Gásquez et al., 2019). In this environment, residual sulfate-bearing fluids were stored in the pore spaces of the altered bedrock, facilitating the precipitation of various sulfate minerals, including prolific gypsum deposits, gypsum foam, and additional varieties such as epsomite, thenardite, mirabilite, jarosite, and natrojarosite (Figs. 14–16). Gypsum flowers, common speleothems, exhibit unique curved or spiral forms driven by episodic variations in $CaSO_4$ solution flow rate and concentration during fibrous or prismatic crystal growth (Ghergari and Onac, 1995). The unusual gypsum foam, not previously documented in other cave systems, displays vibrant colors that may be caused by small amounts of Fe–Mn oxide coatings; however, these oxides were not detected by powder XRD. Epsomite appears as bright green-yellow nodules, whereas mirabilite and thenardite are white powders. These are highly soluble sulfate minerals that are common in sulfuric acid caves and are sensitive to humidity and temperature, with mirabilite altering to thenardite upon exposure to dry air (Hill and Forti, 1997). Sodium and magnesium may have been sourced from evaporite deposits interbedded with gypsum and dolomite in the Toroweap Formation located above the Redwall Limestone (Sorauf and Billingsley, 1991) or, alternatively, could have been sourced from Precambrian felsic igneous and metamorphic rocks located below the Redwall Limestone (Brown et al., 1979; Ilg et al., 1996). Magnesium may have additionally been sourced from interbedded dolomite in the Mooney Falls Member of the Redwall Limestone (Dohm, 2017).

Additionally, other less common minerals, such as jarosite and natrojarosite, precipitated after sulfate-rich waters ceased following the drop in the potentiometric surface, further evidencing this evaporative stage of speleogenesis. These hydroxysulfate minerals, forming in sulfuric acid-rich environments (Kawano and Tomita, 2001), can form directly from the interaction of H_2SO_4 with K, Al, and Fe clays (Polyak and Provencio, 2001; D'Angeli et al., 2018) or can originate from pyrite oxidation or sulfate-rich solutions found in other caves (Hill and Forti, 1997; Audra et al., 2013). The sodium in natrojarosite may derive from halite-bearing Precambrian sedimentary rocks or from igneous rocks with Na-varieties of feldspar (Karlstrom et al., 2012), while potassium sources could include Precambrian sedimentary rocks and clays from the Cambrian Bright Angel Shale (Baldwin et al., 2004). Furthermore, both potassium and sodium are common in breccia pipes with concentrations above average for host formations (Wenrich, 1985). We interpret that the formation of the hydromagnesite deposits also occurred during Stage 4, likely resulting from the dissolution of dolomitic rocks (Hill and Forti, 1997). As groundwater interacts with dolomitic rocks, the Mg/Ca ratio rises, allowing magnesium-rich minerals such as hydromagnesite and magnesite to form (Columbu et al., 2021). Lastly, brushite, a hydrated calcium phosphate, can form via the alteration of bat guano (e.g., Marincea et al., 2004; Audra et al., 2019). The presence of thousands of mummified bats is a unique feature of the BCS (Mead et al., 2021; Chambers et al., 2024), potentially explaining the presence of brushite in this cave system.

APPROXIMATE AGE AND TIMING OF THE BCS STAGES

The BCS currently sits 6.6 km away and 940 m above the Colorado River and is a relict feature of the ancient RM aquifer, which existed before the formation of the Grand Canyon, adding complexity to our understanding of its speleogenetic history. New numerical modeling using multivariate statistical analysis by Ashjari et al. (2024) estimates that it could have taken between 4 and 10 million years for the BCS to develop at depth beneath the water table, which would coincide with the timing of our stages 1 and 2.

Previous hypogene speleogenesis models for Grand Canyon caves have provided important information on the canyon's age and evolution, specifically by Polyak et al. (2008), who dated mammillary formations in Leandras, indicating that the water table was at the elevation of the BCS around 3.5 ± 1.2 Ma. This timeframe suggests that the first two stages of BCS speleogenesis occurred in the phreatic zone before 3.5 ± 1.2 Ma, which is broadly in alignment with the timing inferred from Ashjari et al. (2024), while the third stage began after the water table descended to the level of the BCS.

Modern incision rates from the eastern Grand Canyon of 160 m/Ma (Crow et al., 2014) are temporally stable but spatially variable and indicate it could have taken approximately 5.9 Ma for the water table to drop from the elevation of the BCS to its current level, suggesting that stages 3 and 4 took place during the last 5.9 Ma. However, based on the variable nature of incision rates in the Grand Canyon region, in addition to the U/Pb dates of mammillary formations in Leandras (Polyak et al., 2008), we conclude that stages 3 and 4 likely happened over the past ~4.7 Ma. The stage 4 processes were initiated when the water table dropped completely below the level of the BCS when incision and denudation carved side canyons around the BCS, creating multiple new entrances exposed on opposite sides of canyons, suggesting that previously these would have been throughgoing cave passages that are now crosscut by side canyons. Chambers et al. (2024) radiocarbon dated 67 well-preserved bat specimens from the BCS and found that ages range from modern to >45,800 cal BP, near the practical upper limit of radiocarbon dating; this indicates that the caves were accessible to bats (and therefore open to the surface) for at least ~46 ka. Although stage 4 was likely initiated much earlier than the radiocarbon window, the >45,800 cal BP result provides a minimum age constraint on stage 4 initiation.

HYPOGENE FLUID HETEROGENEITY AND MULTI-PHASE SPELEOGENESIS IN THE GRAND CANYON

The formation of the BCS reflects a complex interplay of tectonic evolution, hydrogeological conditions, and the migration of chemically diverse hypogene fluids. The existing conceptual model for hypogene cave formation in the

Grand Canyon developed by Polyak et al. (2017) provides a valuable framework in which caves formed primarily through the ascent of CO_2-rich fluids under deep phreatic conditions, with sulfuric acid playing a minor role. In this model, speleogenetic byproducts record an ordered sequence of subevents related to regional water table fluctuations and episodic tectonic or magmatic activity.

The BCS shares key elements of this framework, notably the hypogene origin linked to deep-seated fluid ascent in relation to the position of the descending water table. Early phreatic dissolution in the BCS likely occurred under CO_2-rich conditions at depth, consistent with hypogene cave development elsewhere in the Grand Canyon. However, the mineralogical record of the BCS indicates important departures from the existing conceptual model (Table 3).

Most notably, the BCS contains abundant sulfate minerals, including extensive speleogenetic gypsum rinds, indicating that sulfuric acid likely played a major role during one of the later phases of cave development. This contrasts with many previously documented hypogene caves in the Grand Canyon, where limited gypsum abundance suggested a minor role of H_2S. The dominance of sulfate minerals in addition to copper mineralization in the BCS highlights substantial spatial variability in hypogene fluid chemistry across the Grand Canyon.

Additional divergence is evident in the speleogenetic byproducts and secondary mineral deposits preserved in the BCS. Although Polyak et al. (2017) described a progression that includes cave dissolution, Fe and Mn oxides, calcite spar linings, mammillary calcite, folia, cave rafts, and late-stage gypsum rinds, the BCS exhibits some components of this suite, but others have not been identified to date. Calcite spar linings are largely absent (other than locally preserved spar near the Green Door Fault zone), mammillary calcite formations are limited in Leandras and not documented in Double Bopper, and folia and cave rafts are not widely documented, despite the BCS being the largest cave system in the Grand Canyon. Instead, sulfate deposits dominate the secondary mineral assemblage, indicating an altered or incomplete speleogenetic sequence with the potential for overprinting.

The absence of widespread calcite spar linings also bears on estimates of speleogenetic depth. Previous estimates placing cave spar formation at approximately 500 ± 250 m below the water table are based on observations from the unconfined karst system of the Guadalupe Mountains (Decker et al., 2016). In contrast, hypogene cave development in the Grand Canyon likely occurred under initially confined conditions, followed by progressive water table lowering with transition to an unconfined system. As a result, depth estimates derived from unconfined settings may not be directly transferable, and more site-specific hydrogeologic and geochemical modeling is required to constrain speleogenetic depths in the Grand Canyon.

These observations indicate that hypogene speleogenesis in the Grand Canyon is controlled not only by the position of the water table and the contribution of hypogene fluids but also by the pronounced spatial and temporal heterogeneity in fluid sources and migration pathways via faults. Building on the framework of Polyak et al. (2017), our model emphasizes that multiple hypogene fluids of varying origins can mix and react in complex, location-dependent ways, as the evolving fault and fracture network at BCS taps distinct reservoirs and flow paths during magmatic and tectonic events. The BCS demonstrates that no single speleogenetic sequence applies regionally, underscoring the need for a more flexible conceptual model for hypogene cave development in the Grand Canyon.

CONCLUSIONS

The formation of the BCS occurred through the complex interplay of geological and hydrological processes over millions of years. Initially, acidic hypogene fluids circulated through the Redwall Limestone in the deep phreatic zone, dissolving bedrock and creating horizontal passageways. As the environment evolved, fluctuating potentiometric surfaces and changing water chemistries led to the deposition of various minerals, including iron and manganese oxides. The transition to an unconfined evaporative vadose system further contributed to the mineral diversity within the cave, producing speleothems such as gypsum flowers and unique gypsum foam. Subsequent mineral formations, including stalagmites, stalactites, and phosphates from bat guano, reflect the ongoing modern vadose processes within the cave system. This multistage speleogenesis highlights the dynamic interactions between groundwater movement, mineral precipitation, and the geological framework of the Grand Canyon region, ultimately shaping the BCS into the complex cave observed today.

The BCS, recognized as hosting the two largest caves in the Grand Canyon, offers compelling new evidence that broadens existing models of hypogene speleogenesis in the region (Polyak et al., 2017). Our research highlights the influential role of both regional-scale processes and localized geochemical variability in driving cave formation. A key contribution of this study is the emphasis on multifluid interaction in the speleogenesis of the BCS. The cave's development was shaped by the interplay between various hypogenic fluids, specifically carbonic acid, sulfuric acid, and copper-bearing fluids, contributing to remarkable mineralogical diversity, including distinct deposits of malachite, gypsum, and jarosite.

Moreover, our findings underscore the critical importance of recognizing the heterogeneous sources of origin for these fluids in hypogene speleogenesis. The observed variability in fluid contributions is essential for understanding the mechanisms behind mineral deposition and cave morphology, as localized geochemical conditions can greatly influence the variety of unique features within the BCS, setting it apart from other hypogene systems documented in the Grand Canyon. Finally, this study calls for a more integrated approach to hypogene karst research that considers the episodic, regionally variable, and multifluid nature of speleogenesis. Future investigations should prioritize exploring the interplay of multiple fluids and their evolving roles in shaping cave formation processes. This novel understanding of the spatial and temporal heterogeneity of groundwater fluids observed in the BCS not only contributes unique insights to karst literature but also serves as a vital component in advancing our understanding of hypogene caves in both contemporary and ancient systems.

ACKNOWLEDGMENTS

This work is the culmination of over a decade's worth of exploration from numerous citizen scientists in the caving community who have dedicated enormous efforts to map and document the unique resources in the Bopper Cave System. Sample collection was completed with help from James Hunter, Garrison Loope, and Jason Ballensky. Several photographers granted permission for use of their spectacular photos, including Stephen Eginoire, James Hunter, Paul Burger, and Dave Bunnell. We also thank Dr. Joe De Waele, Dr. Augusto Auler, and an anonymous reviewer for the *Journal of Cave and Karst Studies* for their thoughtful, constructive feedback and insightful suggestions that helped improve this manuscript and highlighted directions for future research. This research was conducted under NPS permit GRCA-2021-SCI-0014.

AUTHOR CONTRIBUTION STATEMENT

BT proposed and received funding for the study. SH and BT finalized the study design. SH, BT, and GL collected the samples. SH analyzed the data and wrote the manuscript. BT and GL assisted with interpretation and editing of the manuscript.

REFERENCES

Ashjari, J., Tobin, B., Fryar, A.E., and Ashjari, Z., 2024, Numerical modeling of development of Leandras and Double Bopper Caves, Grand Canyon, USA: Hydrogeology Journal, v. 32, no. 6, p. 1751–1768, https://doi.org/10.1007/s10040-024-02812-z.

Audra, P., Gázquez, F., Rull, F., Bigot, J.-Y., and Camus, H., 2013, Hypogene sulfuric acid speleogenesis and rare sulfate minerals (Fibroferrite, Jarosite subgroup) Baume Galiniere Cave (Alpes-de-Haute-Provence, France), *in* Filippi, M., and Bosák, P., eds., Proceedings of the International Congress of Speleology, 16th, Brno, Czech Republic: Volume 3: Praha, Czech Republic, Czech Speleological Society, p. 432–436.

Audra, P., De Waele, J., Bentaleb, I., Chroňáková, A., Krištůfek, V., D'Angeli, I., Carbone, C., Madonia, G., Vattano, M., Scopelliti, G., Cailhol, D., Vanara, N., Temovski, M., Bigot, J., Nobecourt, J.-C., Galli, E., Rull, F., and Sanz-Arranz, A., 2019, Guano-related phosphate-rich minerals in European caves: International Journal of Speleology, v. 48, no. 1, p. 75–105.

Baldwin, C.T., Strother, P.K., Beck, J.H., and Rose, E., 2004, Palaeoecology of the Bright Angel Shale in the eastern Grand Canyon, Arizona, USA, incorporating sedimentological, ichnological and palynological data, *in* McIlroy, D., ed., *The Application of Ichnology to Palaeoenvironmental and Stratigraphic Analysis*: London, Geological Society, Special Publication 228, p. 213–236, https://doi.org/10.1144/GSL.SP.2004.228.01.11.

Billingsley, G.H., and Hampton, H.M., 2000, Geologip map of the Grand Canyon 30′ x 60′ quadrangle, Coconino and Mohave counties, northwestern Arizona: U.S. Geological Survey Geologic Investigation Series I-2688, version 1.0, scale 1:100,000, p. 15, http://pubs.usgs.gov/imap/i-2688.

Beus, S.S., 1990, Redwall Limestone and Surprise Canyon Formation, *in* Beus, S.S., and Morales, M., eds., *Grand Canyon Geology*: New York, Oxford University Press, p. 119–145.

Blakey, R.C., and Ranney, W., 2008, *Ancient Landscapes of the Colorado Plateau*: Grand Canyon Village, AZ, Grand Canyon Association, p. 156.

Brown, E.H., Babcock, R.S., Clark, M.D., and Livingston, D.E., 1979, Geology of the older Precambrian rocks of the Grand Canyon: Part I: Petrology and structure of the Vishnu Complex: Precambrian Research, v. 8, no. 3–4, p. 219–241, https://doi.org/10.1016/0301-9268(79)90030-5.

Bucher, K., and Stober, I., 2010, Fluids in the upper continental crust: Geofluids, v. 10, no. 1–2, p. 241–253, https://doi.org/10.1111/j.1468-8123.2010.00279.x.

Burgess, S.A., 2021, Sulfur systematics and carbonate diagenesis in the Mitchell Plateau, Indiana [Master's thesis]: Bloomington, Indiana University, 149 p.

Carmichael, M.J., Carmichael, S.K., Santelli, C.M., Strom, A., and Bräuer, S.L., 2013, Mn(II)-oxidizing bacteria are abundant and environmentally relevant members of ferromanganese deposits in caves of the upper Tennessee river basin: Geomicrobiology Journal, v. 30, no. 9, p. 779–800, https://doi.org/10.1080/01490451.2013.769651.

Chambers, C.L., Thomas, S., Santucci, V.L., Oswald, H., and Ballensky, J., 2024, Ancient bat remains illustrate the role of caves as habitat anchors in the temporally dynamic landscape of the Grand Canyon: Parks Stewardship Forum, v. 40, no. 1, p. 39–52, https://doi.org/10.5070/P540162920.

Columbu, A., Audra, P., Gázquez, F., D'Angeli, I.M., Bigot, J.-Y., Koltai, G., Chiesa, R., Yu, T.-L., Hu, H.-M., Shen, C.-C., Carbone, C., Heresanu, V., Nobécourt, J.-C., and De Waele, J., 2021, A hypogenic cave system with late-stage condensation-corrosion and epigenic overprinting (Toirano, Liguria, Italy): Geomorphology, v. 376, p. 107561, https://doi.org/10.1016/j.geomorph.2020.107561.

Crossey, L.J., Fischer, T.P., Patchett, P.J., Karlstrom, K.E., Hilton, D.R., Newell, D.L., Huntoon, P., Reynolds, A.C., and de Leeuw, G.A.M., 2006, Dissected hydrologic system at the Grand Canyon: Interaction between deeply derived fluids and plateau aquifer waters in modern springs and travertine: Geology, v. 34, no. 1, p. 25–28, https://doi.org/10.1130/G22057.1.

Crossey, L.J., Karlstrom, K.E., Springer, A.E., Newell, D., Hilton, D.R., and Fischer, T., 2009, Degassing of mantle-derived CO_2 and He from springs in the Southern Colorado Plateau region-Neotectonic Connections and implications for groundwater systems: Geological Society of America Bulletin, v. 121, no. 7–8, p. 1034–1053, https://doi.org/10.1130/B26394.1.

Crow, R., Karlstrom, K.E., McIntosh, W., Peters, L., and Dunbar, N., 2008, History of quaternary volcanism and lava dams in Western Grand Canyon based on lidar analysis, $^{40}Ar/^{39}Ar$ dating, and field studies: Implications for flow stratigraphy, timing of volcanic events, and lava dams: Geosphere, v. 4, no. 1, p. 183–206, https://doi.org/10.1130/GES00133.1.
Crow, R., Karlstrom, K., Darling, A., Crossey, L., Polyak, V., Granger, D., Asmerom, Y., and Schmandt, B., 2014, Steady incision of Grand Canyon at the million year timeframe: A case for mantle-driven differential uplift: Earth and Planetary Science Letters, v. 397, p. 159–173, https://doi.org/10.1016/j.epsl.2014.04.020.
D'Angeli, I., Carbone, C., Nagostinis, M., Parise, M., Vattano, M., Madonia, G., and De Waele, J., 2018, New insights on secondary minerals from Italian sulfuric acid caves: International Journal of Speleology, v. 47, no. 3, p. 271–291.
De Waele, J., Audra, P., Madonia, G., Vattano, M., Plan, L., D'Angeli, I.M., Bigot, J., and Nobécourt, J-C., 2016, Sulfuric acid speleogenesis (SAS) close to the water table: Examples from southern France, Austria, and Sicily: Geomorphology, v. 253, 452–467, https://doi.org/10.1016/j.geomorph.2015.10.019.
De Waele, J., D'Angeli, I.M., Audra, P., Plan, L., and Palmer, A.N., 2024, Sulfuric acid caves of the world: A review: Earth-Science Reviews, v. 250, p. 104693, https://doi.org/10.1016/j.earscirev.2024.104693.
Decker, D.D., Polyak, V.J., and Asmerom, Y., 2016, A supercritical CO_2 hypogene speleogenesis model: The origin of spar caves and cave spar in the Guadalupe Mountains, USA, *in* Chavez, T., and Reehling, P., eds., *Proceedings of DeepKarst 2016*: Carlsbad, NM, April 11–14: National Cave and Karst Research Institute, p. 21–25.
Dohm, P.W., 2017, A sequence stratigraphic analysis of the Mooney Falls Member of the Redwall Limestone [Bachelor's thesis]: Durango, Fort Lewis College, 45 p.
DuChene, H.R., Palmer, A.N., Palmer, M.V., Michael Queen, J., Polyak, V.J., Decker, D.D., Hill, C.A., Spilde, M., Burger, P.A., Kirkland, D.W., and Boston, P., 2017, Hypogene speleogenesis in the Guadalupe Mountains, New Mexico and Texas, USA, *in* Klimchouk, A., Palmer, A.N., De Waele, J., Auler, A.S., and Audra, P., eds., *Hypogene Karst Regions and Caves of the World*: Cham, Springer, p. 511–530, https://doi.org/10.1007/978-3-319-53348-3_31.
Farrant, A.R., and Harrison, T., 2017, Hypogenic caves in the UK, *in* Klimchouk, A., Palmer, A.N., De Waele, J., Auler, A.S., and Audra, P., eds., *Hypogene Karst Regions and Caves of the World*: Cham, Springer, p. 43–60, https://doi.org/10.1007/978-3-319-53348-3_2.
Galdenzi, S., Jones, D.S., and Macalady, J.L., 2014, Condensation corrosion: Measurements and geomorphic evidence in the Frasassi caves, *in* Klimchouk, A., Sasowsky, I.D., Mylroie, J., Engel, S.A., and Engel, A.S., eds., *Hypogene Cave Morphologies*: Karst Waters Institute, Inc., Leesburg, VA, Karst Waters Institute Special Publication 18, Karst Waters Institute, Inc., p. 44–46.
Gásquez, F., Calaforra, J.M., Evans, N.P., Turchyn, A.V., Rull, F., Medina, J., Ros, A., Llamusi, J.L., Sanchez, J.A.R., and Hodell, D.A., 2019, Physical weathering of carbonate host-rock by precipitation of soluble salts in caves: A case study in El Oron-Arco Cave (Region of Murcia, SE Spain): Chemical Geology, v. 521, p. 1–11, https://doi.org/10.1016/j.chemgeo.2019.05.010.
Ghergari, L., and Onac, B.-P., 1995, The crystallogenesis of gypsum flowers: Cave and Karst Science, v. 22, no. 3, p. 119–122.
Gulley, J.D., and Polk, J.S., 2017, Hypogene karst influences in the Upper Floridan aquifer, *in* Klimchouk, A., Palmer, A.N., De Waele, J., Auler, A.S., and Audra, P., eds., *Hypogene Karst Regions and Caves of the World*: Cham, Springer, p. 745–755, https://doi.org/10.1007/978-3-319-53348-3_50.
Heimel, S., 2019, Matrix porosity controls on karst morphology in the Mooney Falls Member of the Redwall Limestone of the Grand Canyon [Bachelor's thesis]: Durango, Fort Lewis College, 25 p., https://doi.org/10.13140/RG.2.2.16292.35206.
Heimel, S., 2022, Hypogene speleogenesis in the Grand Canyon: Observational, mineralogical, and geochemical investigations from the Bopper Cave System [Master's thesis]: Lexington, University of Kentucky, 105 p, https://doi.org/10.13023/etd.2023.025.
Heimel, S.M., and Tobin, B.W., 2022, Geospatial applications of cave resource data to better understand epikarst and unsaturated zone groundwater flow path development: Geosciences, v. 12, no. 2, p. 47, https://doi.org/10.3390/geosciences12020047.
Hill, C.A., 1990, Sulfuric acid speleogenesis of Carlsbad Cavern and its relationship to hydrocarbons, Delaware basin, New Mexico and Texas: American Association of Petroleum Geologists Bulletin, v. 74, no. 11, p. 1685–1694.https://doi.org/10.1306/0C9B2565-1710-11D7-8645000102C1865D.
Hill, C.A., and Forti, P., 1997, *Cave Minerals of the World* (2nd edition): Huntsville, AL, National Speleological Society, p. 463.
Hill, C.A., and Polyak, V.J., 2010, Karst hydrology of Grand Canyon, Arizona, USA: Journal of Hydrology, v. 390, no. 3–4, p. 169–181, https://doi.org/10.1016/j.jhydrol.2010.06.040.
Hose, L.D., DuChene, H.R., Jones, D., Baker, G.M., Havlena, Z., Sweetkind, D., and Powell, D., 2021, Hypogenic karst of the Great Basin, *in* Florsheim, J., Koeberl, C., McKay, M.P., and Riggs, N., eds., *Field Excursions from the 2021 GSA Section Meetings: Geological Society of America Field Guide 61*: Boulder, CO, The Geological Society of America (GSA), p. 77–114, https://doi.org/10.1130/2020.0061(05).
Huntoon, P.W., 1974, The karstic groundwater basins of the Kaibab Plateau, Arizona: Water Resources Research, v. 10, no. 3, p. 579–590, https://doi.org/10.1029/WR010i003p00579.
Huntoon, P.W., 1996, Large-basin ground water circulation and paleo-reconstruction of circulation leading to uranium mineralization in Grand Canyon breccia pipes, Arizona: The Mountain Geologist, v. 33, no. 3, p. 71–84.
Huntoon, P.W., 2000a, *Karstification Associated with Groundwater Circulation Through the Redwall Artesian Aquifer*: Grand Canyon, AR, National Speleological Society.
Huntoon, P.W., 2000b, Variability of karstic permeability between unconfined and confined aquifers, Grand Canyon region, Arizona: Environmental and Engineering Geoscience, v. 6, no. 2, p. 155–170, https://doi.org/10.2113/gseegeosci.6.2.155.
Ilg, B.R., Karlstrom, K.E., Hawkins, D.P., and Williams, M.L., 1996, Tectonic evolution of Paleoproterozoic rocks in the Grand Canyon: Insights into middle-crustal processes: Geological Society of America Bulletin, v. 108, no. 9, p. 1149–1166, https://doi.org/10.1130/0016-7606(1996)108≤1149:TEOPRI≥2.3.CO;2.
Jones, C.J.R., 2017, Characterization of the Redwall–Muav aquifer of the Grand Canyon and Kaibab Plateau, Arizona, based on Roaring Springs hydrograph analysis [Master's thesis]: Flagstaff, Northern Arizona University, 151 p.
Karlstrom, K.E., Timmons, J.M., and Crossey, L.J., 2012, Introduction to Grand Canyon geology, *in* Timmons, M.J., and Karlstrom, K.E., eds., *Grand Canyon Geology: Two Billion Years of Earth's History*: Boulder, CO, Geological Society of America, https://doi.org/10.1130/2012.2489(00).
Karlstrom, K.E., Lee, J.P., Kelley, S.A., Crow, R.S., Crossey, L.J., Young, R.A., Lazear, G., Beard, L.S., Ricketts, J.W., Fox, M., and Shuster, D.L., 2014, Formation of the Grand Canyon 5 to 6 million years ago through integration of older palaeocanyons: Nature Geoscience, v. 7, no. 3, p. 239–244, https://doi.org/10.1038/ngeo2065.

Karlstrom, K.E., Wilgus, J., Thacker, J.O., Schmandt, B., Coblentz, D., and Albonico, M., 2022, Tectonics of the Colorado Plateau and its margins: Annual Review of Earth and Planetary Sciences, v. 50, no. 1, p. 295–322, https://doi.org/10.1146/annurev-earth-032320-111432.
Kawano, M., and Tomita, K., 2001, Geochemical modeling of bacterially induced mineralization of Schwertmannite and Jarosite in sulfuric acid spring water: American Mineralogist, v. 86, no. 10, p. 1156–1165, https://doi.org/10.2138/am-2001-1005.
Kent, W.N., and Rawson, R.R., 1980, Depositional environments of the Mississippian Redwall Limestone in northeastern Arizona, *in* Fouch, T.D., and Magathan, E.R., eds., *Proceedings, Rocky Mountain Paleogeography Symposium, 1st*: Denver, CO, Society of Economic Paleontologists and Mineralogists, Rocky Mountain Section, p. 101–109.
Klimchouk, A., and Ford, D., 2000, Lithologies and structural controls of dissolutional cave development, *in* Bottrell, S.H., Gunn, J., Lowe, D.J., Klimchouk, A.B., Ford, D.C., Palmer, A.N., and Dreybrodt, W., eds., *Speleogenesis: Evolution of Karst Aquifers*: Huntsville, AL, National Speleological Society, p. 54–64.
Klimchouk, A., 2009, Morphogenesis of hypogenic caves: Geomorphology, v. 106, no. 1–2, p. 100–117, https://doi.org/10.1016/j.geomorph.2008.09.013.
Klimchouk, A., 2012, Speleogenesis, hypogenic, *in* White, W.B., and Culver, D.C., eds., *Encyclopedia of Caves* (2nd edition): Waltham, MA, Academic Press, p. 748–765, https://doi.org/10.1016/B978-0-12-383832-2.00110-9.
Klimchouk, A., Palmer, A.N., De Waele, J., Auler, A.S., and Audra, P., eds., 2017, *Hypogene Karst Regions and Caves of the World*: Cham, Springer, p. 911, https://doi.org/10.1007/978-3-319-53348-3.
Levy, D.B., 2007, Oxidation-reduction chemistry of Lechuguilla Cave seepage: Journal of Cave and Karst Studies, v. 69, no. 3, p. 351–358.
Mandl, G., 2005, *Rock Joints: The Mechanical Genesis*: Berlin, Springer, p. 230, https://doi.org/10.1007/b137623.
Marincea, S., Dumitraş, D.-G., Diaconu, G., and Bilal, E., 2004, Hydroxylapatite, brushite and ardealite in the bat guano deposit from Peştera Mare de la Mereşti, Perşani Mountains, Romania, Neues Jahrbuch fur Mineralogie Monatshefte, v. 10, p. 464–488.
McKee, E.D., 1963, Nomenclature for lithologic subdivisions of the Mississippian Redwall Limestone, Arizona: U.S. Geological Survey Professional Paper 475-C, p. C21–C22, https://doi.org/10.3133/pp475C.
McKee, E.D., and Gutschick, R.C., 1969, History of the Redwall Limestone of northern Arizona: Geological Society of America Memoir, v. 114, p. 726, https://doi.org/10.1130/MEM114-p1.
Mead, J.I., Tweet, J.S., Santucci, V.L., Tobin, B., Chambers, C.L., Thomas, S.C., and Carpenter, M.C., 2021, Pleistocene/Holocene cave fossils from Grand Canyon National Park-Ice Age (Pleistocene) flora, fauna, environments, and climate of the Grand Canyon, Arizona, *in* Santucci, V.L., and Tweet, J.S., eds., *Grand Canyon National Park Centennial Paleontological Resource Inventory—A Century of Fossil Discovery and Research*: Utah Geological Association Special Publication 1, p. 221–240.
Melchiorre, E.B., and Enders, M.S., 2003, Stable isotope geochemistry of copper carbonates at the Northwest Extension Deposit, Morenci District, Arizona: Implications for conditions of supergene oxidation and related mineralization: Economic Geology, v. 98, no. 3, p. 607–621, https://doi.org/10.2113/98.3.607.
Palmer, A.N., 1975, The Origin of Maze Caves: NSS Bulletin, v. 37, no. 3, p. 57–76.
Palmer, A.N., 1991, Origin and morphology of limestone caves: Geological Society of America Bulletin, v. 103, no. 1, p. 1–21, https://doi.org/10.1130/0016-7606(1991)103<0001:OAMOLC>2.3.CO;2.
Palmer, A.N., 2007, *Cave Geology*: Dayton, Ohio, Cave Books, 454 p.
Palmer, A.N., Palmer, M.V., and Paces, J.B., 2016, Geologic history of the Black Hills caves, South Dakota, *in* Feinberg, J.M., Gao, Y., and Alexander, E.C., eds., *Caves and Karst Across Time*: Geological Society of America Special Paper 516, p. 87–101, https://doi.org/10.1130/2015.2516(07).
Palmer, M.V., and Palmer, A.N., 2012, Petrographic and isotopic evidence for late-stage processes in sulfuric acid caves of the Guadalupe Mountains, New Mexico, USA: International Journal of Speleology, v. 41, no. 2, p. 231–250, https://doi.org/10.5038/1827-806X.41.2.10.
Pegler, S.S., Huppert, H.E., and Neufeld, J.A., 2014, Fluid migration between confined aquifers: Journal of Fluid Mechanics, v. 757, p. 330–353, https://doi.org/10.1017/jfm.2014.469.
Polyak, V., Hill, C., and Asmerom, Y., 2008, Age and evolution of the Grand Canyon revealed by U–Pb dating of water table-type speleothems: Science, v. 319, no. 5868, p. 1377–1380, https://doi.org/10.1126/science.1151248.
Polyak, V.J., Hill, C.A., Asmerom, Y., and Decker, D.D., 2017, A conceptual model for hypogene speleogenesis in Grand Canyon, Arizona, *in* Klimchouk, A., Palmer, A.N., De Waele, J., Auler, A.S., and Audra, P., eds., *Hypogene Karst Regions and Caves of the World*: Cham, Springer, p. 555–564, https://doi.org/10.1007/978-3-319-53348-3_34.
Polyak, V.P., and Provencio, P., 2001, By-product materials related to H_2S-H_2SO_4 influenced speleogenesis of Carlsbad, Lechuguilla, and other caves of the Guadalupe Mountains, New Mexico: Journal of Cave and Karst Studies, v. 63, no. 1, p. 23–32.
Roberts, G.G., White, N.J., Martin-Brandis, G.L., and Crosby, A.G., 2012, An uplift history of the Colorado Plateau and its surroundings from inverse modeling of longitudinal river profiles: Tectonics, v. 31, no. 4, p. 27, https://doi.org/10.1029/2012TC003107.
Sorauf, J.E., and Billingsley, G.H., 1991, Members of the Toroweap and Kaibab Formations, Lower Permian, northern Arizona and southwestern Utah: The Mountain Geologist, v. 28, no. 1, p. 9–24.
Spötl, C., Desch, A., Dublyansky, Y., Plan, L., and Mangini, A., 2016, Hypogene speleogenesis in dolomite host rock by CO_2 rich fluids, Kozak Cave (southern Austria): Geomorphology, v. 255, p. 39–48, https://doi.org/10.1016/j.geomorph.2015.12.001.
Spötl, C., Plan, L., and Dublyansky, Y., 2017, Hypogene karst in Austria, *in* Klimchouk, A., Palmer, A.N., De Waele, J., Auler, A.S., and Audra, P., eds., *Hypogene Karst Regions and Caves of the World*: Cham, Springer, p. 113–126, https://doi.org/10.1007/978-3-319-53348-3_6.
Sylvia, D.A., 1985, Depositional, diagenetic, and subsidence history of the Redwall Limestone, Grand Canyon National Park, Arizona [Master's thesis]: Tucson, University of Arizona, 265 p.
Tennyson, R., Brahana, V., Polyak, V.J., Potra, A., Covington, M., Asmerom, Y., Terry, J., Pollock, E., and Decker, D.D., 2017, Hypogene speleogenesis in the southern Ozark uplands, mid-continental United States, *in* Klimchouk, A., Palmer, A.N., De Waele, J., Auler, A.S., and Audra, P., eds., *Hypogene Karst Regions and Caves of the World*: Cham, Springer, p. 663–676, https://doi.org/10.1007/978-3-319-53348-3_43.
Tobin, B.W., Springer, A.E., Ballensky, J., and Armstrong, A., 2021, Cave and karst of the Grand Canyon World Heritage Site: Zeitschrift Für Geomorphologie, v. 62, no. 3, p. 125–144, https://doi.org/10.1127/zfg_suppl/2021/0693.
Wells, N.A., Waugh, D.A., and Foos, A.M., 2003, Some notes and hypotheses concerning iron and iron remobilization features in the Sharon Formation (Summit County, Ohio), *in* Foos, A.M., ed., *Pennsylvanian Sharon Formation, Past and Present: Sedimentology, Hydrogeology, and Historical and Environmental Significance: Ohio Division of Geological Survey Guidebook* 18: Columbus, OH, Department of Natural Resources, Division of Geological Survey, p. 33–37.

Wenrich, K.J., 1985, Mineralization of breccia pipes in northern Arizona: Economic Geology, v. 80, no. 6, p. 1722–1735, https://doi.org/10.2113/gsecongeo.80.6.1722.

Wenrich, K.J., and Sutphin, H.B., 1989, *Lithotectonic setting necessary for formation of a uranium-rich, solution-collapse Breccia-Pipe Province, Grand Canyon Region*: Arizona, U.S. Geological Survey Open-File Report 89-0173.

White, W.B., and White, E.L., 2003, Gypsum wedging and cavern breakdown: Studies in the Mammoth Cave System, Kentucky: Journal of Cave and Karst Studies, v. 65, no. 1, p. 43–52.